

Microwave-assisted synthesis of Mg:PbI_2 nanostructures and their structural, morphological, optical, dielectric and electrical properties for optoelectronic technology

Mohd. Shkir, Ziaul Raza Khan, T Alshahrani, Kamlesh V. Chandekar, M Aslam Manthrammel, Ashwani Kumar, S AlFaify

Citation: Chin. Phys. B . 2020, 29(11): 116102 . **doi:** 10.1088/1674-1056/aba60e
Journal homepage: http://cpb.iphy.ac.cn; http://iopscience.iop.org/cpb

What follows is a list of articles you may be interested in

Effects of 3d-transition metal doping on the electronic and magnetic properties of one-dimensional diamond nanothread

Zhenzhen Miao(苗珍珍), Can Cao(曹粲), Bei Zhang(张蓓), Haiming Duan(段海明), Mengqiu Long(龙孟秋)

Chin. Phys. B . 2020, 29(6): 066101 . **doi:** 10.1088/1674-1056/ab84dd

Structural and electronic properties of transition-metal chalcogenides Mo_5S_4 nanowires

Ming-Shuai Qiu(邱明帅), Huai-Hong Guo(郭怀红), Ye Zhang(张也), Bao-Juan Dong(董宝娟), Sajjad Ali(阿里.萨贾德), Teng Yang(杨腾)

Chin. Phys. B . 2019, 28(10): 106103 . **doi:** 10.1088/1674-1056/ab3f9a

Van der Waals interlayer potential of graphitic structures: From Lennard-Jones to Kolmogorov-Crespy and Lebedeva models

Zbigniew Koziol, Grzegorz Gawlik, Jacek Jagielski

Chin. Phys. B . 2019, 28(9): 096101 . **doi:** 10.1088/1674-1056/ab38a5

Zn-Cu-codoped SnO_2 nanoparticles:Structural, optical, and ferromagnetic behaviors

Syed Zulfiqar, Zainab Iqbal, Jianguo Lü(吕建国)

Chin. Phys. B . 2017, 26(12): 126104 . **doi:** 10.1088/1674-1056/26/12/126104

High-pressure structural properties of tetramethylsilane

Zhen-Xing Qin(秦振兴) and Xiao-Jia Chen(陈晓嘉)

Chin. Phys. B . 2016, 25(2): 026104 . **doi:** 10.1088/1674-1056/25/2/026104

Microwave-assisted synthesis of Mg:PbI_2 nanostructures and their structural, morphological, optical, dielectric and electrical properties for optoelectronic technology*

Mohd. Shkir[1,†], Ziaul Raza Khan[2], T Alshahrani[3], Kamlesh V. Chandekar[4], M Aslam Manthrammel[1], Ashwani Kumar[5], and S AlFaify[1]

[1] *Advanced Functional Materials and Optoelectronics Laboratory (AFMOL), Department of Physics, College of Science, King Khalid University, Abha* 61413, *P.O. Box* 9004, *Saudi Arabia*

[2] *Department of Physics, College of Science, University of Hail, P.O. Box* 2440, *Hail, Saudi Arabia*

[3] *Department of Physics, College of Science, Princess Nourah Bint Abdulrahman University, Riyadh* 11671, *Saudi Arabia*

[4] *Department of Physics, Rayat Shikshan Sanstha's, Karmaveer Bhaurao Patil College, Vashi, Navi Mumbai* 400703, *India*

[5] *Department of Physics, IK Gujral Punjab Technical University, Jalandhar* 144603, *India*

(Received 23 May 2020; revised manuscript received 7 July 2020; accepted manuscript online 15 July 2020)

This work reports the cost-effective growth of Mg:PbI_2 nanostructures with 0, 1, 2.5 and 5.0 wt.% Mg doping concentrations. Structural, vibrational, morphological properties are analyzed using x-ray diffraction (XRD), Raman spectroscopy and scanning electron microscopy (SEM). XRD and Raman studies confirm the monophasic hexagonal system of Mg:PbI_2, and no additional impurity peaks are detected. The Scherrer formula is used to determine sizes of crystallites to be in the range of 47–52 nm. EDX/SEM e-mapping analyses confirm the incorporation of Mg in PbI_2 matrix and its uniform distribution throughout the sample. The hexagonal nanosheet- and nanoplate-like morphologies are detected in SEM images for pure and Mg-doped PbI_2. An optical band gap of nanostructures is obtained from Tauc's relation to be in the range 3.0–3.25 eV. Dielectric and electrical properties are found in significant enhancement as Mg doping in PbI_2 matrix, also the conduction mechanism is discussed.

Keywords: Mg:PbI_2 nanostructures, structural properties, optical band gap, dielectric constant, ac conductivity

PACS: 61.46.–w, 03.75.Hh, 78.67.–n, 87.19.rf **DOI:** 10.1088/1674-1056/aba60e

1. Introduction

Lead iodide nanostructures have been drawn a great deal of attention from researchers for decades mainly owing to their excellent nuclear radiation detection and photovoltaic properties.[1–9] PbI_2 is a metal-halide semiconductor material with direct band gap 2.40 eV at room temperature. It has an anisotropic layered structure with $P\bar{3}1$ space group and structural parameters $a = b = 4.56$ Å, $c = 6.98$ Å, $\alpha = \beta = 90°$, $\gamma = 120°$.[10,11] In addition, PbI_2 nanoplates, nanowires and nanostructures have been widely used to fabricate flexible and highly sensitive photodetector devices.[7,12–14] Recently, lead iodide enables the new role in the development of highly efficient perovskite solar cells. Because lead iodide ability is to react with amine iodides such as methyl ammonium iodide to produce halide perovskites such as $CH_3NH_3PbI_3$ with significant optoelectronics properties. Therefor, PbI_2 nanostructures grown by a cost effective method can be a promising candidate to synthesize perovskite materials for optoelectronics applications.[6,15–19] PbI_2 nanostructures have also been grown with various elements such as Zn, La, Hg, Nd, Au, Ag, and Mn.[20–26] Mg-doped PbI_2 nanostructures were grown using a facile microwave assisted chemical route method and their structural, electronic structure and dielectric and electrical properties have been rarely studied. Various techniques such as chemical precipitating, hydrothermal, sol-gel and microwave assisted chemical precipitation methods have been employed to develop PbI_2 nanostructures.[27–34] In this paper, we focus on the growth of Mg:PbI_2 nanostructures with different Mg-doping concentrations 0, 1, 2.5, and 5.0 wt.% using the facile microwave assisted method and investigate their structural, vibrational, morphological, optical, dielectric and electrical properties for optoelectronics applications.

2. Experimental procedure

To achieve nanostructures of Mg:PbI_2, we have procured lead acetate, sodium iodide (NaI), magnesium nitrate hexahydrate, sodium dodecyl sulfate (SDS), and acetic acid from Sigma Aldrich. In a typical process, 0.5 M lead acetate was taken in 4 cylindrical glass vessels and dissolved with 50 ml of DDW at 70 °C on a hot plate with a magnetic stirrer under regular stirring at 700 rpm for about 15 min, then 0.5 g or 50 ml of SDS solution was added from stock solution. Also 25 ml of acetic acid was added to make the solution transparent. Then to dope Mg we have added 0.0, 1.0, 2.5 and 5.0 wt.% of mag-

*Project supported by the Deanship of Scientific Research at King Khalid University (Grant No. R.G.P1/207/41), the Deanship of Scientific Research at Princess Nourah bint Abdulrahman University through the Fast-track Research Funding Program, and Deanship of Research, University of Hail.

†Corresponding author. E-mail: shkirphysics@gmail.com

© 2020 Chinese Physical Society and IOP Publishing Ltd

nesium nitrate hexahydrate and stirring was carried out under similar conditions. Finally, the prepared solutions of 1 M of sodium iodide (NaI) under similar conditions were added and we observed that all the solutions started to become yellow, which signifies the synthesis of PbI_2 and no other color was seen in final products after 1 h continuous stirring. All solutions were then subjected to microwave irradiation for 15 min of time at 700 W power using a domestic microwave system. All the samples were washed with about 2 L of DDW and then the powder was collected and dried at 80 °C in an oven.

3. Results and discussion

4. Phase confirmation

Phase confirmation of Mg:PbI_2 nanostructures grown by the microwave assisted method with different Mg doping concentrations was carried out by XRD measurement using a Shimadzu LabX-6000 x-ray diffractometer. Figure 1(a) reveals that the as-grown nanostructures are polycrystalline in nature. The prominent peak of PbI_2 was centered along (101) plane at $2\theta \sim 25.905°$.[35–37] An additional indexed family of planes located at (001), (100), (002), (101), etc. confirms that the grown Mg:PbI_2 nanostructures have a hexagonal crystalline structure, which agrees closely with the JCPDS card No. 07-0235.[38] All diffractograms are displayed in Fig. 1, exhibiting the pure phase of PbI_2 nanostructures. However, exotic effect of Mg doping can be seen noticeably from Fig. 1(b). As Pb atoms replaced by Mg atoms in the PbI_2 matrix, the characteristic peak centered along (001) plane shows reduction in intensity of peak and increase in FWHM of the peak along with shift in peak position. It may be due to the difference of atomic size of the Pb atom from the Mg atom. Atomic radii of Pb and Mg atoms are 119 and 72 pm, respectively. This peak shift may be attributed to (1) changes in stoichiometric composition by doping, (2) microstructure parameters (crystallize size and lattice strain) and (3) thermal annealing. The peak shifting due to the chemical pressure is caused by the change in lattice parameters as per Vegard's law and Shannon–Prewitt radii. From Fig. 1(b), we can observe that the XRD peak of as-prepared samples shifts towards the lower angle side with increasing the doping contents. The decrease in the diffracting angle would increase the lattice parameters for hexagonal crystal structures as suggested by the following equations:

$$c = \frac{\lambda}{\sin\theta}, \tag{1}$$

$$a = \frac{\lambda}{\sqrt{3}\sin\theta}. \tag{2}$$

From Eqs. (1) and (2), it is observed that the lattice parameters are inversely proportional to the diffraction angle θ. Thus, decrease in the diffraction angle on increasing dopant content would increase both the lattice parameters and hence, the volume of a unit cell of the hexagonal crystal structure increases with increase in dopant contents, which can be confirmed by

$$V = \frac{\sqrt{3}}{2}a^2c. \tag{3}$$

In addition, we have performed Rietveld refinements of the XRD patterns for detailed analyses. Microstructures parameters (crystallite size and local random lattice strain) generally result in broadening of XRD peaks and do not contribute to shifting.

Hence, the crystalline quality of PbI_2 nanostructures becomes degraded with incorporation of Mg in PbI_2 matrix. The effects of different element doping concentrations on PbI_2 nanostructures have been reported earlier by various researchers.[14,23,24,39] The crystal size of nanostructures was obtained using Debye Scherer's empirical relation $D_{101} = k\lambda/\beta\cos\theta$, and crystallite sizes were in order of 47–51 nm. Lattice constants, dislocation density and strain of nanostructures were estimated experimentally from the following well-known relations:[40–42]

$$\frac{1}{d^2} = \frac{4}{3}\left[\frac{h^2+hk+k^2}{a^2}\right] + \frac{l^2}{c^2}, \tag{4}$$

$$\delta_{101} = \frac{1}{D_{101}^2}, \tag{5}$$

$$\varepsilon_{101} = \frac{\beta\cot\theta}{4}. \tag{6}$$

Lattice constant values a and c are found in close agreement with the JCPDS#7-0235, and the structural parameters are listed in Table1. The values of lattice constants were found to increase with the increase in Mg doping concentration. Rietveld refinement of recorded XRD spectra of Mg:PbI_2 nanostructures with different Mg concentrations are shown in Figs. 1(c)–1(f). Rietveld refinement shows the growth of nanostructures along (101) plane and the similar behavior of lattice constants was observed from the recorded XRD patterns.

Table 1. Refined structural constraints for all Mg:PbI_2 by POWDERX software and Rietveld refinement processes.

Sample	POWDERX software			Rietveld refined			D_{101}/nm	$\delta_{101}/10^{-4}$ nm^{-2}	$\varepsilon_{101}/10^{-3}$
$Pb_{1-x}Mg_xI_2$	a/Å	c/Å	V/Å^3	a/Å	c/Å	V/Å^3			
JCPSD#7-0235	4.5570	6.9790	125.5100	–	–	–	–	–	–
$x = 0.0$ wt.%	4.5572	6.9786	125.5160	4.5556	6.9767	125.3918	51.23	3.81	3.02
$x = 1.0$ wt.%	4.5577	6.9778	125.5310	4.5578	6.9812	125.5946	49.25	4.12	3.15
$x = 2.5$ wt.%	4.5574	6.9803	125.5605	4.5550	6.9769	125.3650	48.20	4.30	3.21
$x = 5.0$ wt.%	4.5590	6.9822	125.6817	4.5553	6.9782	125.4019	47.47	4.44	3.27

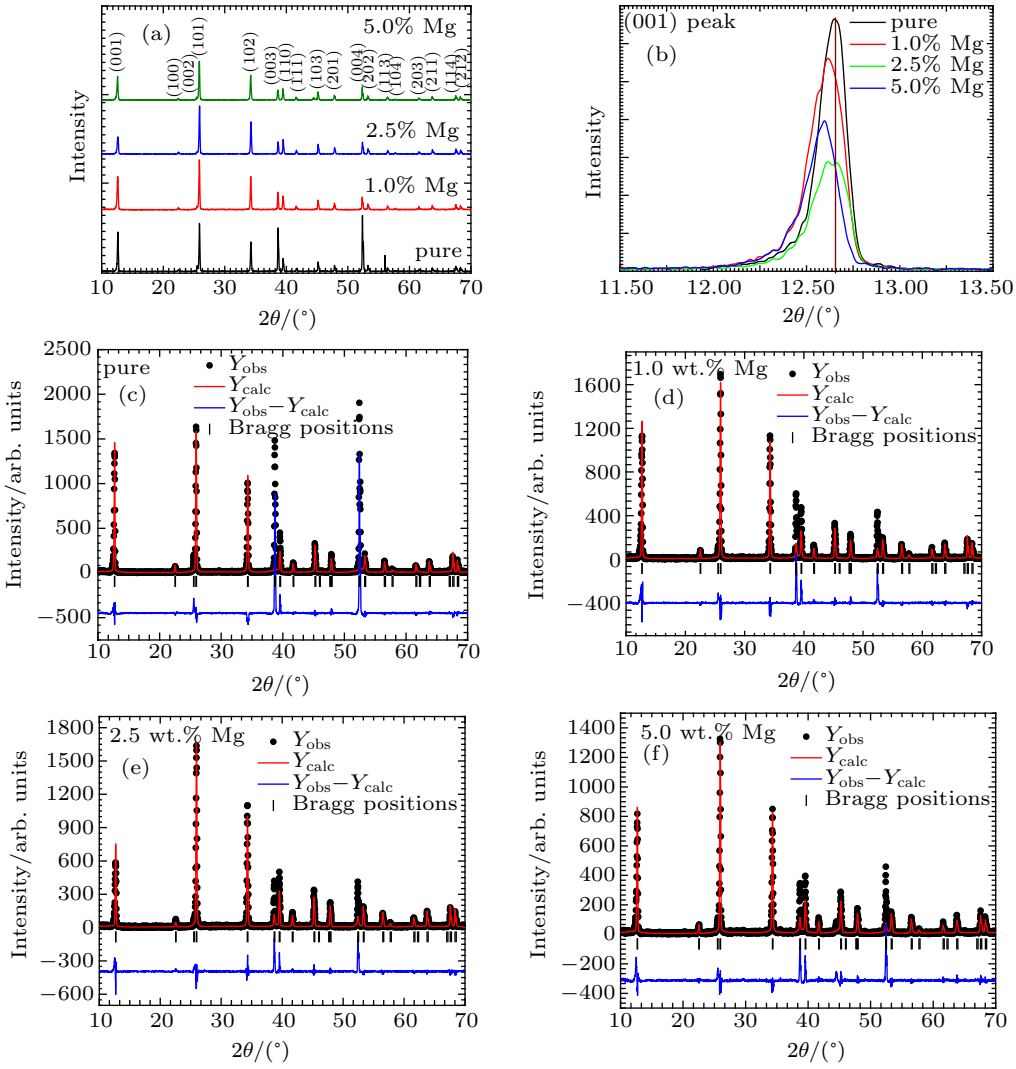


Fig. 1. (a) As-recorded XRD patterns, (b) close view of the (001) peak, (c)–(f) Rietveld refined XRD patterns for pure and Mg-doped PbI_2 nanostructures.

4.1. Vibrational spectroscopy

Figure 2 illustrates the measured FT-Raman spectrum of Mg:PbI_2 nanostructures with different doping concentrations using a DXR FT-RAMAN spectrometer having 532 nm laser operated at 0.2 mW. As shown in Fig. 2, the vibrational modes of spectra suggested that the as-grown Mg:PbI_2 nanostructures are found highly pure materials. The characteristic bands of PbI_2 are centered at 73.13, 96, 111, 164, 213 cm^{-1}, which correspond to vibration modes such as $E2_1$, $A1_1$, $A1_2$, $2E_1^2$ and $2E_1^1$, respectively. Similar results of vibration modes of PbI_2 were reported by some research groups earlier.[43,44] The effect of Mg doping can be observed clearly from Fig. 2. The intensity and FWHM of peaks were enhanced as the Mg atom replacing in PbI_2 matrix along with shift in peak positions. The shifting in peak positions confirms the variation of nanostructure sizes with Mg doping concentrations, which is in agreement closely with the XRD results.

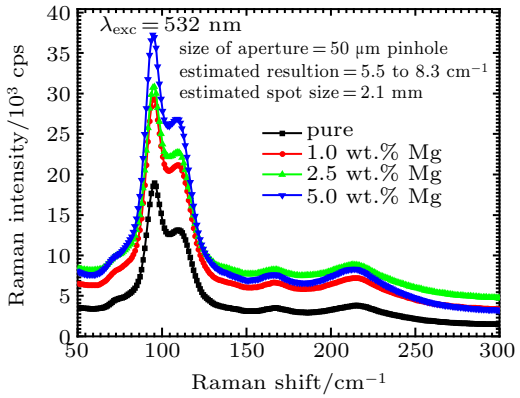


Fig. 2. FT-Raman spectra for pure and Mg-doped PbI_2.

4.2. Elemental composition and morphology analyses

Figures 3(a)–3(b) show the EDX and SEM e-mapping of the as-grown Mg:PbI_2 nanostructures doped with 2.5 wt.% Mg recorded with a JEOL 6360 SEM/EDX system. The sample shows a good stoichiometric ratio which is confirmed from Fig. 3(a) and tabulated in the inset. It can be concluded that the Mg atom successfully replaced the Pb atom in PbI_2 matrix, which has been approved from XRD and Raman stud-

ies. In addition, Fig. 3(b) shows the uniform distribution of Mg atoms in PbI_2 matrix. Effect of Mg doping on the nanostructure morphology were investigated using SEM. Figures 4(a)–4(d) depict SEM images of Mg:PbI_2 nanostructures with different doing concentrations. Figure 4(a) illustrates the clear hexagonal sheet-type nanostructures. As Mg doping concentration increases, morphology of nanostructures becomes nanoplate-type structures, as seen noticeably from Figs. 4(b)–4(d). Nanosheet- and Nanoplate-like morphologies were also observed earlier in Cd:PbI_2.[45]

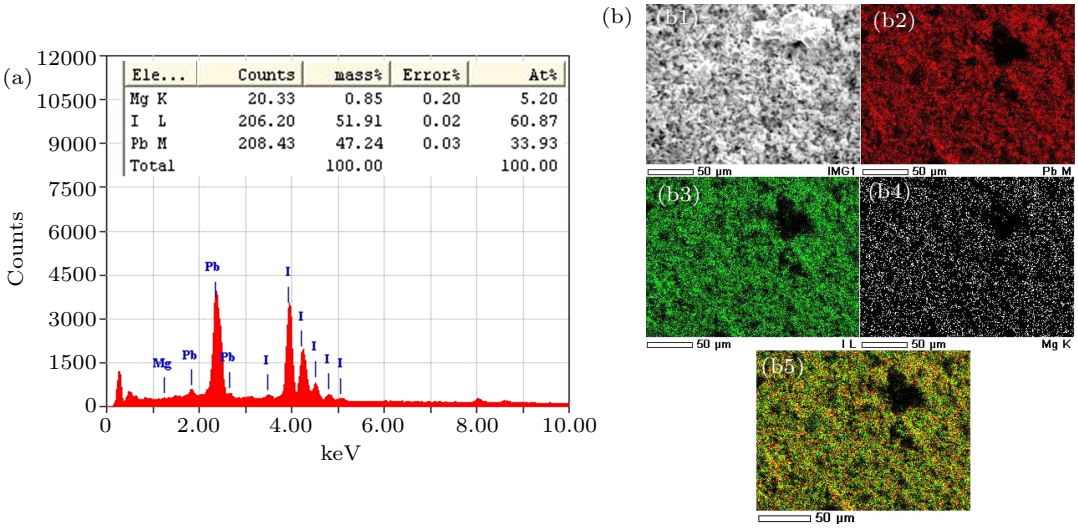


Fig. 3. EDX spectra with composition and (b) SEM e-mapping images for 2.5 wt.% Mg:PbI_2.

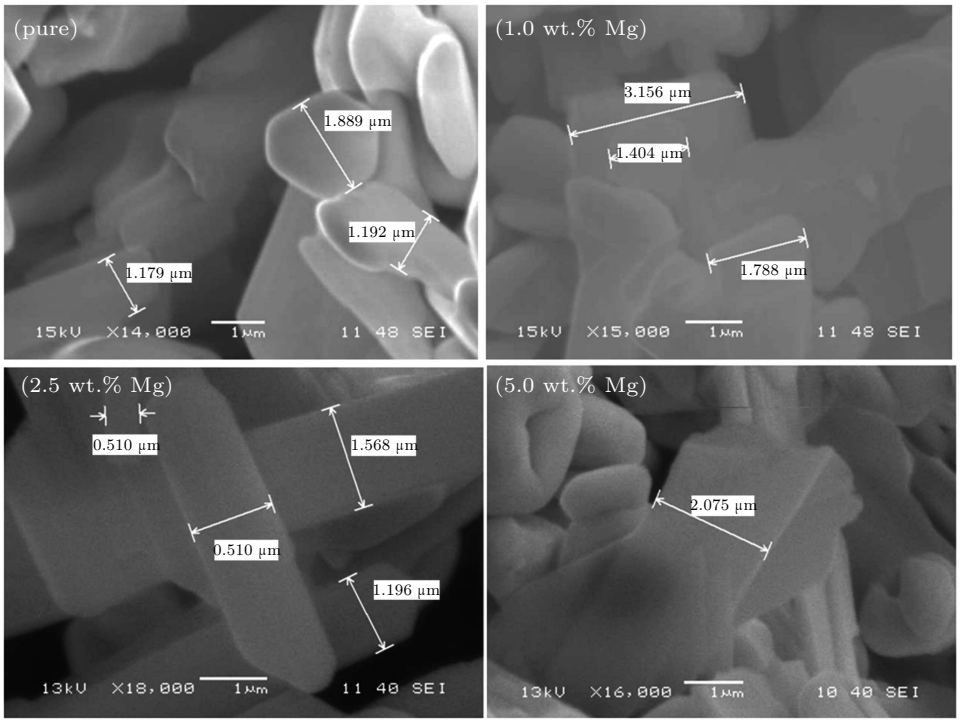


Fig. 4. SEM micrographs for pure and Mg-doped PbI_2.

4.3. Band gap evaluation

Electronic structure of nanostructures with different Mg doping concentrations were investigated using UV-vis absorbance spectra recorded with a JASCO V570 UV-Vis spectrometer for dispersed Mg:PbI_2 nanostructures in water. Figure 5(a) shows the absorbance spectra of as-grown nanostructures in the range 300–900 nm. The band gaps were determined using Tauc's relation:[45,46] $\alpha h\nu = A(h\nu - E_g)^m$, where A is the transition characteristic parameter; h, ν, and E_g are the Plank constant, frequency of light, optical band gap, respectively; and m is a parameter describing the type of transition process. Tauc's plot of Mg:PbI_2 nanostructures with different Mg doping concentrations is shown in Fig. 5(b). Extracted values of the nanostructure optical band gap from Fig. 5(b) are

in the range 3.0–3.25 eV. Already, significant effects of Mg doping concentrations on structural and morphological properties of nanostructures have been confirmed in the above section, which directly influence band structure of the material. Doping may affect the optical band gap to become higher or lower. Firstly, the optical band gap increases or decreases according to the density of localized states, i.e., becoming lower or higher. XRD and SEM are useful techniques to produce the details of localized states. At 1.0 wt.% Mg, the intensity of XRD becomes greater with reduced FWHM value compared to other doping contents. This provides enhancement in crystalline order and the localized states or reduction in defects, which means the enhancement in the crystallite size (see Table 1).

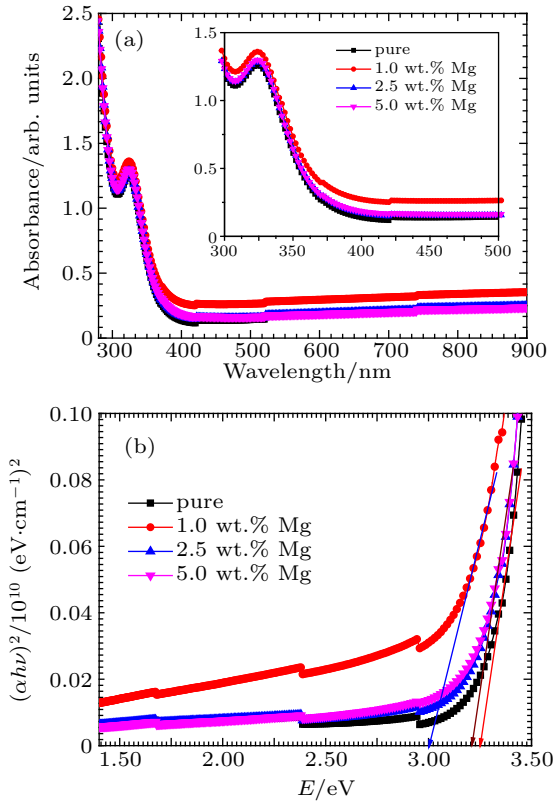


Fig. 5. (a) Absorbance plot and (b) Tauc's plot for Mg:PbI_2.

We can see that the 1.0 wt.% Mg-doped PbI_2 sample under SEM has irregularly shaped morphologies. Here, crystallites are growing to form nanoplates but not completely. Therefore, irregularly shaped morphologies were observed in SEM images. However, nanoplates were formed in certain sizes in the 2.5 wt.% Mg sample and the same type of nanoplates was also observed in the 5.0 wt.% Mg sample with increased sizes compared to the former. Thus, the higher the crystallite size, the random shapes in the morphology of crystals with larger sizes, and the more the broadening of the valence band. The conduction band is formed to exhibit a reduction of optical band value at 1.0 wt.% Mg compared to 2.5 and 5.0 wt.% Mg.[47] Here, an optical band gap of nanostructures was decreased with Mg doped in PbI_2 matrix. Effect of Mg doping on optical band gap of PbI_2 nanostructures is difficult to find in literature. However, various researchers have been reported effects of different elements doping except Mg on optical band gaps of PbI_2 nanostructures such as Cd and Zn, and band gap engineering is reported in PbI_2.[45,48,49] Narrowing of band gap was also observed in Cr:PbI_2, Dy:PbI_2, Mg/Cd:ZnO, etc.[50–53]

4.4. Capacitive storage and electrical properties

Dielectric constant of Mg:PbI_2 nanostructures as a function of frequency in the range from 3 kHz to 10 MHz is shown in Fig. 6(a), prior to this a KEITHLEY 4200-SCS setup was employed to record C, Z and $\tan\delta$ in mentioned frequency region. A lot of earlier reported works on dielectric constants of semiconductor nanostructure materials have been shown higher dielectric constant values than bulk counterparts.[54] High dielectric materials exhibited potential application in super capacitors, cost effective field effect transistors and gate dielectric materials.[55–57] Frequency dependent dielectric constants are usually measured using a bridge type capacitance measurement system used to obtain the complex frequency-dependent dielectric constant given by the relation $\varepsilon^* = \varepsilon' - \mathrm{i}\varepsilon''$, where ε' and ε'' are real and imaginary parts of dielectric constant, respectively. The dielectric constant can be estimated using the relation $\varepsilon' = Cd/A\varepsilon_0 A$ and dielectric loss calculated via the relation $\varepsilon'' = \varepsilon' \times \tan\delta$.

Figure 6(a) reveals a significant behavior of dielectric constant as a function of frequency, throughout the range of frequency the value of dielectric constant is almost unchanged. This confirms that the dielectric constant behavior does not obey electric field. However, noticeable enhancement in dielectric constant values can be seen from Fig. 6(a) with Pb replaced with Mg in PbI_2 matrix. In addition, the value of dielectric constant is found to be higher than the bulk PbI_2 crystal[58,59] and comparable to nanostructured PbI_2.[45,48]

Figure 6(b) illustrates the dielectric loss of the Mg:PbI_2 nanostructures as a function of frequency. In lower frequency region, the loss is higher than that in higher frequency region. This may be due to the fact that electric dipoles can pursue electric field. Overall, dielectric loss is very low, which confirms the grown Mg:PbI_2 nanostructures pure and defect free. Total ac conductivity of nanostructures was recorded using the notorious relation $\sigma_{\mathrm{ac.tot}} = d/ZA$, where d, A and Z are the thickness, area and impedance of samples, respectively.

Figure 6(c) displays the total ac conductivity as a function of frequency. The ac conductivity of nanostructures increases gradually in lower frequency region and sudden tends to higher values in higher frequency region. Further, investigation of conduction mechanism of nanostructures in Jonscher's

theory[60] was adopted: $\sigma_{ac.tot} \approx B\omega^s$, where B is constant, ω is the angular frequency and s is frequency exponent. From Fig. 6(c), it can be observed that the nanostructures obey universal frequency law. The value of exponent s was obtained using Fig. 6(c) and found to be in the range 0.9958–0.9989, which is smaller than 1, suggesting that the charge carried mechanism is according to the CBH model. Noticeable enhancement in ac conductivity was observed as Mg doping in the PbI_2 system. Overall dielectric and electrical investigation of Mg:PbI_2 nanostructures suggests that it is a potential candidate for super capacitor and optoelectronics applications.

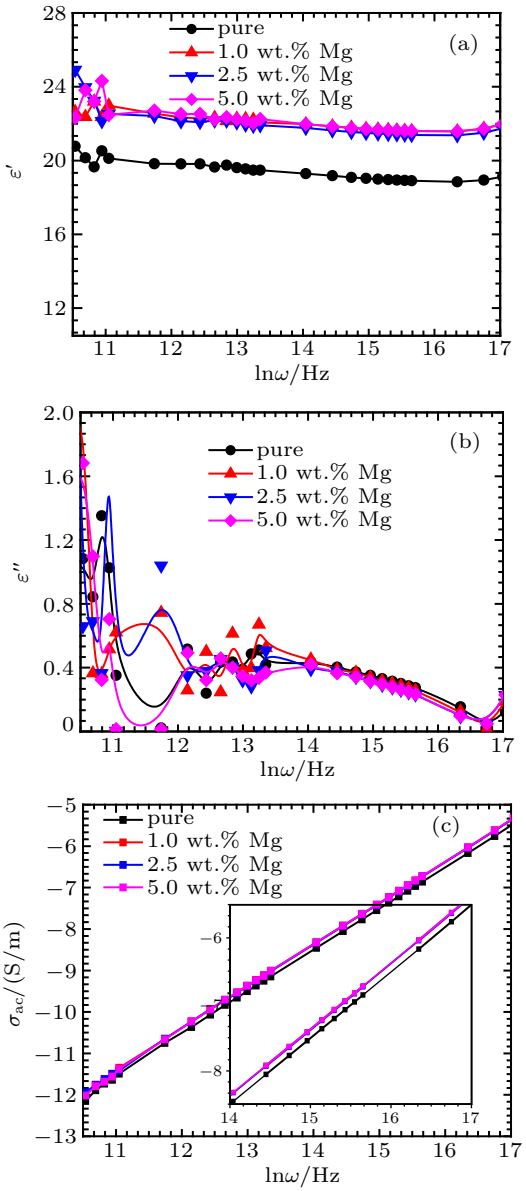


Fig. 6. Graphics for (a) ε' vs $\ln\omega$, (b) ε'' vs $\ln\omega$, and (c) σ_{ac} vs $\ln\omega$ for all Mg:PbI_2 samples.

5. Conclusions

Mg:PbI_2 nanostructures with different Mg doping concentrations have been synthesized by a microwave assisted cost effective method. XRD analyses of nanostructures reveal that as-grown nanostructures have a hexagonal structure with single phase. Lattice constant and dislocation density of samples increase with the increase in Mg doping concentration. SEM analyses of nanostructures show the significant effect of doping on morphologies of nanostructures. The pure-sample SEM image reveals that clear hexagonal sheets as Mg incorporates in PbI_2 matrix morphology become of hexagonal nanoplates. The band gap of nanostructures decreases with the increase in Mg doping concentration. Dielectric constant of nanostructures increases from 20 to 24 as Mg doping concentration increases. Conduction mechanism signifies that there is charge transport involving the CBH model. Our investigation strengthens the reliability of Mg:PbI_2 nanomaterials for opto-dielectric applications.

References

[1] Kojima A, Teshima K, Shirai Y and Miyasaka T 2009 *J. Am. Chem. Soc.* **131** 6050
[2] Jiang Q, Zhao Y, Zhang X, Yang X, Chen Y, Chu Z, Ye Q, Li X, Yin Z and You J 2019 *Nat. Photon.* **13** 460
[3] Sun H, Zhao B, Zhu X, Zhu S, Yang D, Wangyang P and Gao X 2018 *Appl. Surf. Sci.* **427** 1146
[4] Shah K, Street R, Dmitriyev Y, Bennett P, Cirignano L, Klugerman M, Squillante M and Entine G 2001 *Nucl. Instrum. Methods A* **458** 140
[5] Mo J, Zhang C, Chang J, Yang H, Xi H, Chen D, Lin Z, Lu G, Zhang J and Hao Y 2017 *J. Mater. Chem. A* **5** 13032
[6] Leal D A A, Krishnan B, Shaji S and Avellaneda D A 2018 *Mater. Chem. Phys.* **215** 137
[7] Zhang J, Huang Y, Tan Z, Li T, Zhang Y, Jia K, Lin L, Sun L, Chen X, Li Z, Tan C, Zhang J, Zheng L, Wu Y, Deng B, Chen Z, Liu Z and Peng H 2018 *Adv. Mater.* **30** 1803194
[8] Shah K S, Olschner F, Moy L P, Bennett P, Misra M, Zhang J, Squillante M R and Lund J C 1996 *Nucl. Instrum. Methods A* **380** 266
[9] Al-Daraghmeh T M, Saleh M H, Ahmad M J A, Bulos B N, Shehadeh K M and Jafar M M A G 2018 *J. Electron. Mater.* **47** 1806
[10] Shkir M, Abbas H and Khan Z R 2012 *J. Phys. Chem. Solids* **73** 1309
[11] Ferreira da Silva A, Veissid N, An C, Pepe I, Barros de Oliveira N and Batista da Silva A 1996 *Appl. Phys. Lett.* **69** 1930
[12] Zhong M, Zhang S, Huang L, You J, Wei Z, Liu X and Li J 2017 *Nanoscale* **9** 3736
[13] Qi Z, Yang T, Li D, Li H, Wang X, Zhang X, Li F, Zheng W, Fan P, Zhuang X and Pan A 2019 *Mater. Horizns* **6** 1474
[14] Ismail R A, Mousa A M and Shaker S S 2019 *Opt. Quantum Electron.* **51** 362
[15] Chen Y, Zhang L, Zhang Y, Gao H and Yan H 2018 *RSC Adv.* **8** 10489
[16] Gujar T P, Unger T, Schönleber A, Fried M, Panzer F, van Smaalen S, Köhler A and Thelakkat M 2018 *Phys. Chem. Chem. Phys.* **20** 605
[17] Kim H S, Lee C R, Im J H, Lee K B, Moehl T, Marchioro A, Moon S J, Humphry-Baker R, Yum J H and Moser J E 2012 *Sci. Rep.* **2** 591
[18] Xiao M, Huang F, Huang W, Dkhissi Y, Zhu Y, Etheridge J, Gray-Weale A, Bach U, Cheng Y B and Spiccia L 2014 *Angew. Chem. Int. Ed.* **53** 9898
[19] Duong T, Mulmudi H K, Shen H, Wu Y, Barugkin C, Mayon Y O, Nguyen H T, Macdonald D, Peng J and Lockrey M 2016 *Nano Energy* **30** 330
[20] Mohammed S I, Shanshool H M and Imhan K I 2019 *J. Theor. Appl. Phys.* **13** 269
[21] Khan M T, Shkir M, Almohammedi A and AlFaify S 2019 *Solid State Sci.* **90** 95
[22] AlFaify S, Shkir M and Ganesh V 2018 *Mater. Sci. Semicond. Process.* **83** 231
[23] Shkir M and AlFaify S 2017 *Sci. Rep.* **7** 16091
[24] Shkir M, Yahia I S, Ganesh V, Bitla Y, Ashraf I M, Kaushik A and AlFaify S 2018 *Sci. Rep.* **8** 13806
[25] Abutalib M and Yahia I 2017 *J. Mol. Struct.* **1138** 215
[26] Al-Douri Y, Hashim U, Bouhemadou A and Ameri M 2015 *Nanoelectron. Optoelectron.* **10** 705

[27] Mohammed S I and Al-Douri Y 2014 *Advanced Materials Research* (Durnten-Zurich: Trans Tech Publications Ltd) Vol. 925 pp. 164–168
[28] Shkir M, AlFaify S, Yahia I S, Hamdy M S, Ganesh V and Algarni H 2017 *J. Nanopart. Res.* **19** 328
[29] Barnakov Y A, Ito S, Dmitruk I, Tsunekawa S and Kasuya A 2001 *Scr. Mater.* **45** 273
[30] Finlayson C and Sazio P 2006 *J. Phys. D: Appl. Phys.* **39** 1477
[31] Zhu G, Liu P, Hojamberdiev M, Zhou J-p, Huang X, Feng B and Yang R 2010 *Appl. Phys. A* **98** 299
[32] Ma D, Zhang W, Zhang R, Zhang M, Xi G and Qian Y 2005 *Nanosci. Nanotechnol.* **5** 810
[33] Mu R, Tung Y, Ueda A and Henderson D 1996 *J. Phys. Chem. A* **100** 19927
[34] Tang Z K, Nozue Y and Goto T 1995 *Mater. Sci. Eng. B* **35** 410
[35] Khan Z R, Shkir M, Khan A, Mariappan S M, Balaji M, Sheikh M R and AlFaify S 2020 *Solid State Sci.* **103** 106192
[36] Shkir M, Khan M T and AlFaify S 2019 *Appl. Nanosci.* **9** 1417
[37] Shkir M and AlFaify S 2019 *J. Mater. Res.* **34** 2765
[38] Silva Filho J M C d, Borrero N F V, Viana G A, Merlo R B and Marques F C 2020 *Cryst. Growth* **20** 1531
[39] Yahia I S, Shkir M, Ganesh V, Abutalib M M, Zahran H Y and Alfaify S 2018 *Mater. Sci.-Poland* **36** 320
[40] Khan Z R, Zulfequar M and Khan M S 2010 *Mater. Sci. Eng. B* **174** 145
[41] Shkir M, Khan A, Hamdy M and AlFaify S 2020 *Mater. Res. Express* **6** 1250e6
[42] Shkir M, Chandekar K V, Khan A, El-Toni A M and AlFaify S 2020 *Mater. Sci. Semicond. Process.* **107** 104807
[43] Khilji M, Sherman W and Wilkinson G 1982 *J. Raman Spectrosc.* **13** 127
[44] Wangyang P, Sun H, Zhu X, Yang D and Gao X 2016 *Mater. Lett.* **168** 68
[45] AlFaify S and Shkir M 2019 *Opt. Mater.* **88** 417
[46] Khan Z R, Aziz A and Khan M S 2018 *Mater. Sci.-Poland* **36** 235
[47] Khodja S, Touam T, Chelouche A, Boudjouan F, Djouadi D, Hadjoub Z, Fischer A and Boudrioua A 2014 *Superlattice Microst.* **75** 485
[48] Alfaify S and Shkir M 2019 *J. Nanoelectron. Optoelectron.* **14** 255
[49] Wang Y, Sun Y Y, Zhang S, Lu T M and Shi J 2016 *Appl. Phys. Lett.* **108** 013105
[50] Khan M T, Shkir M, Yahia I S, Almohammedi A and AlFaify S 2020 *Superlattice Microst.* **138** 106370
[51] Quan Z, Liu X, Qi Y, Song Z, Qi S, Zhou G and Xu X 2017 *Appl. Surf. Sci.* **399** 751
[52] Jule L T, Dejene F B, Ali A G, Roro K T, Hegazy A, Allam N K and El Shenawy E 2016 *J. Alloys Compd.* **687** 920
[53] Shkir M, Khan A, El-Toni A M, Aldalbahi A, Yahia I S and AlFaify S 2019 *J. Phys. Chem. Solids* **130** 189
[54] Slonopas A, Ryan H and Norris P 2019 *Electrochim. Acta* **307** 334
[55] Khan Z R, Zulfequar M and Khan M S 2011 *J. Mater. Sci.* **46** 5412
[56] Kumar R and Engles D 2016 *Mater. Today* **3** 1933
[57] Takeya J, Yamagishi M, Tominari Y and Nakazawa Y 2007 *Solid State Electron.* **51** 1338
[58] Glasser L, Hall P and Liebenberg D 1967 *J. Chem. Soc. A* Issue 2 p. 295
[59] Dugan A and Henisch H 1967 *J. Phys. Chem. Solids* **28** 971
[60] Jonscher A K 1977 *Nature* **267** 673